

Dominant Resonance in Parametric Subharmonic Instability of Internal Waves

Y. Liang¹, L.-A. Coustou², Q. C. Guo³, and M.-R. Alam^{*1,3}

¹Applied Science and Technology, University of California Berkeley, Berkeley, CA 94720

²CNRS, Aix Marseille Univ, Centrale Marseille, IRPHE, Marseille, France

³Department of Mechanical Engineering, University of California Berkeley, Berkeley, CA 94720

Abstract

Parametric Subharmonic Instability (PSI) is one of the most important mechanisms that transfer energy from tidally-generated long internal waves to short steep waves. Breaking of these short waves results in diapycnal mixing through which oceanic abyssal stratification is maintained. It has long been believed that PSI is strongest between a primary internal wave and perturbative waves of half the frequency of the primary wave. Here, we rigorously show that this is not the case. Specifically, we show that neither the initial growth rate nor the maximum long-term amplification occur at the half frequency, and demonstrate that the dominant subharmonic waves have much longer wavelengths than previously thought.

1 Introduction

Internal gravity waves are ubiquitous in world's density-stratified oceans. They mainly arise from barotropic tides flowing over topographic features, or wind disturbing the upper ocean's mixed layer [1]. Internal waves transport energy over long distances in oceans and when break result in considerable mixing which contributes to, e.g., oceanic circulations through lifting cold water from the ocean basin [2], and the lives of a wide range of ocean creatures by redistributing nutrients [3, 4].

The underlying mechanism(s) that lead to the breaking of internal waves is not yet fully understood despite significant recent progresses made in our understanding of such waves. There is a nearly general consensus that low mode internal waves, such as those generated by tides, need to somehow transfer their energy to shorter waves which are steeper and hence more prone to breaking. Several mechanisms for such transfer of energy from long to short waves have been put forward, among them interaction with topographic features [5, 6, 7] and parametric subharmonic instability [e.g. 8, 9, 10] are the most important ones.

Parametric Subharmonic Instability (PSI) is the instability of a primary internal wave to two lower-frequency internal waves with (initially) infinitesimal amplitudes thus *disturbances*. This happens if the primary and the two disturbance waves' frequencies and wavenumber vectors (respectively $\omega_{0,1,2}$ and $\mathbf{k}_{0,1,2}$) satisfy the triad resonance condition [e.g. 11, 12, 13]

$$\omega_0 = \omega_1 + \omega_2, \quad \mathbf{k}_0 = \mathbf{k}_1 + \mathbf{k}_2. \quad (1)$$

Through this instability, energy is transferred from the primary wave to the two disturbance waves. The flow of energy may continue until the amplitudes of the disturbance waves, initially infinitesimal, become of the same order as the amplitude of the primary wave or even higher, and that is why the disturbance waves are said to be *resonated*. This resonance is not through an explicit external force but instead is caused by what appears to

*reza.alam@berkeley.edu

be *parameters* in the governing equations, hence it is called *parametric* resonance or instability¹. Resonated subharmonic waves obtained through PSI usually have smaller vertical and horizontal scales than the primary wave. Thus, PSI constitutes a pathway for energy transfer to steeper waves which are more prone to breaking. PSI was first studied [in 1960s, e.g. 8, 9] as a subset of the general wave resonance theory [15, 16], and has since been reported in several field studies [e.g. 17, 18]. The current understanding of PSI is based on a linear stability theory [established in the 1970s, e.g. 19, 20]. Assuming that the amplitude of the primary wave is constant, and that amplitudes of disturbance waves are much smaller than the primary wave, the linear stability theory predicts an exponential growth rate for a pair of perturbing waves that satisfy the resonance conditions (1) [see e.g. 19, 13, 21].

An internal wave, however, can undergo parametric subharmonic instability simultaneously with a countably infinite pairs of subharmonic waves. In order to accurately determine the role of PSI on the evolution of oceanic internal wave spectrum as well as to answer how efficiently an internal wave can transfer its energy to smaller scales, it is critical to know which specific pair (or pairs) of disturbance waves draw the most energy from the primary internal wave. In other words, it is critical to know which triads are resonated the strongest out of all the different triad resonance possibilities. The classical linear stability theory assumes that these infinite resonance possibilities are independent (or decoupled) and predicts that the pair of subharmonic waves with half of the frequency of the primary wave has the largest growth rates and thus is expected to dominate in the process of PSI [e.g. 22, 21].

However, laboratory and numerical experiments on PSI do not support the predominance of half frequency resonant waves. For example, in a series of experiments on PSI in a wave tank 21m long, 1.2m deep and filled with linearly stratified fluid, Martin et al. [19] obtained multiple subharmonic waves generated from PSI of a mode-three internal wave, but none of them were at the half frequency. In another attempt, Joubaud et al. [23] sends a horizontally propagating mode-one internal wave at frequency $0.95N$ (N : Brunt-Väisälä frequency) but observes two subharmonic waves not at the half frequency but at frequencies $0.38N$ and $0.57N$. Also, direct simulation of internal beams generated by a tidal flow (frequency ω_0) over bottom topography results in strongest subharmonic waves at frequencies $0.4\omega_0$ and $0.6\omega_0$ [24].

To address this discrepancy, here we consider the fully-coupled governing interaction equations that account for all triads satisfying PSI resonance condition (1). We solve this governing equation through multiple-scale analysis that obtains a uniformly-valid nonlinear instability solution. Our analysis determines that, contrary to linear stability theory prediction, it is a pair of subharmonic waves with frequencies *different from* $\omega_0/2$ that grow the largest in the PSI. In fact, in cases pairs of frequency $\omega_0/2$ receive the least amount of energy compared to other pairs in the pool of interactions.

Furthermore, internal waves with frequencies near $\omega_0/2$, as can be derived from equation (1), have very large vertical wavenumbers and therefore are very short. In fact, at exactly $\omega_0/2$, the vertical wavenumber is infinite. Strongest resonant waves of PSI, as predicted by the nonlinear stability theory, have frequencies far from ω_0 hence have finite wavenumbers. Therefore, nonlinear stability theory shows that the actual strongest resonant waves of PSI have much larger scales than what linear stability theory predicts.

While it is not unexpected that nonlinear theory results in a long-term growth which is different from the linear theory predictions, it is obvious that both linear and nonlinear theories must give the same initial growth rates. But, to our surprise, our initial growth rate from nonlinear stability theory did not match the prevalent linear growth rate reported in the literature. After some scrutiny we realized that in the classical theory the effect of the second exponential term has been mistakenly neglected, resulting in an incorrect reported initial growth rate. Specifically, in linear stability analysis, amplitude growth in a resonance is usually obtained in the form $A = ae^{bt} + ce^{-bt}$, and therefore the growth rate is $(1/A)(dA/dt) = b(ae^{bt} - ce^{-bt})/(ae^{bt} + ce^{-bt})$. While at large times (at which linear stability analysis is usually not valid) the growth rate tends to b , the initial growth rate is $b[1 - 2c/(a + c)]$, that depends on a, c and can potentially be very much different from b .

In what follows, we present our nonlinear stability analysis and discuss both initial growth rate and overall long-time growth of each resonance triads. We validate our analytical solution with direct numerical simulation results obtained from non-hydrostatic Navier-Stokes solver MITgcm.

¹Some literature [e.g. 14], to be precise, call this resonance a “Parametric Subharmonic instability or PSI” only if the disturbance waves have a frequency half of the frequency of primary wave. If the disturbance waves have a different frequency, then it is called “Triadic Resonant Instability or TRI”.

2 Interaction Equations for Parametric Subharmonic Instability

Consider an inviscid, incompressible and stably-stratified fluid bounded by a top rigid lid and a flat seafloor at the bottom. In a Cartesian coordinates system with x, y -axes on the rigid lid and z -axis positive upward, the governing equations read

$$\rho_0 \mathcal{D}\mathbf{u}/\mathcal{D}t = -\nabla p - \rho g \nabla z, \quad -h < z < 0, \quad (2a)$$

$$\mathcal{D}\rho/\mathcal{D}t = 0, \quad -h < z < 0, \quad (2b)$$

$$\nabla \cdot \mathbf{u} = 0, \quad -h < z < 0, \quad (2c)$$

$$w = 0, \quad z = 0, \quad (2d)$$

$$w = 0, \quad z = -h, \quad (2e)$$

where $\mathbf{u} = \{u, v, w\}$ is the velocity vector, ρ is the density, p is the pressure, and g is the gravitational acceleration. A linear density profile is considered such that the background density is given by $\bar{\rho}(z)/\rho_0 = 1 - az$, with $\rho_0 = \bar{\rho}(z)|_{z=0}$. Equation (2a) is the momentum equation, (2b) represents conservation of salt (assuming that the density only depends on salinity in the equation of state and diffusion of salt is negligible), (2c) is conservation of mass, and equations (2d),(2e) are kinematic boundary conditions on the rigid lid and the sea bottom respectively.

System of equations (2) admits, among other solutions, a propagating internal-wave solution. Considering that a primary internal wave (\mathbf{k}_0, ω_0) with a finite initial amplitude co-exists with two perturbation waves (\mathbf{k}_1, ω_1) and (\mathbf{k}_2, ω_2) the vertical velocity to the leading order can be written in the form

$$w = \sum_{j=0,1,2} A_j \sin m_j(z+h) e^{i(k_j x - \omega_j t)} + \text{c.c.} \quad (3)$$

where $\mathbf{k}_j = k_j \hat{i} + m_j \hat{z}$, and c.c. denotes the complex conjugates. If triad resonance condition (1) is satisfied between the three waves, then amplitudes A_j will slowly change with time. Mathematically this is expressed by $A_j = A_j(\varepsilon t)$, that is, amplitudes are functions of *slow time* (ε is a small parameter and a measure of the waves' steepness).

Let's first define the following dimensionless variables

$$A_j^* = \frac{A_j}{A_{00}}, \quad t^* = \frac{t}{T_0} \cdot \frac{A_{00} T_0}{h}, \quad \omega_j^* = \frac{\omega_j}{N}, \quad k_j^* = k_j h, \quad m_j^* = m_j h.$$

where $A_{00} = A_0(t)|_{t=0}$. Through multiple-scale perturbation analysis, the differential equation that governs the evolution of a wave triad can be obtained, dropping all asterisks, as

$$dA_0(t)/dt = s_0 A_1(t) A_2(t) \quad (4a)$$

$$dA_1(t)/dt = s_1 A_0(t) \bar{A}_2(t) \quad (4b)$$

$$dA_2(t)/dt = s_2 A_0(t) \bar{A}_1(t) \quad (4c)$$

where $\bar{A}_{1,2}(t)$ are complex conjugates of $A_{1,2}(t)$, and²

$$s = \frac{(k_1 m_2 - k_2 m_1)}{4k_0 k_1 k_2} \left(\frac{k_1}{\omega_1} - \frac{k_2}{\omega_2} \right) \left(\frac{k_0}{\omega_0} + \frac{k_1}{\omega_1} + \frac{k_2}{\omega_2} \right) \omega_0^2. \quad (5)$$

The interaction coefficients for the two perturbing waves s_1 and s_2 can be obtained by simply swapping the physical parameters in the expression for s_0 in (5) [c.f. e.g. 25, 21].

²Our equation (5) is in fact the same as (3.26) presented in [21] except for the pre-factor 1/4 which is due to [21] considering a vertically unbounded domain whereas in our study we have vertical wall boundaries. Therefore, in our case, unlike [21], we must have standing waves in the vertical direction and also can only have discrete vertical wavenumbers m .

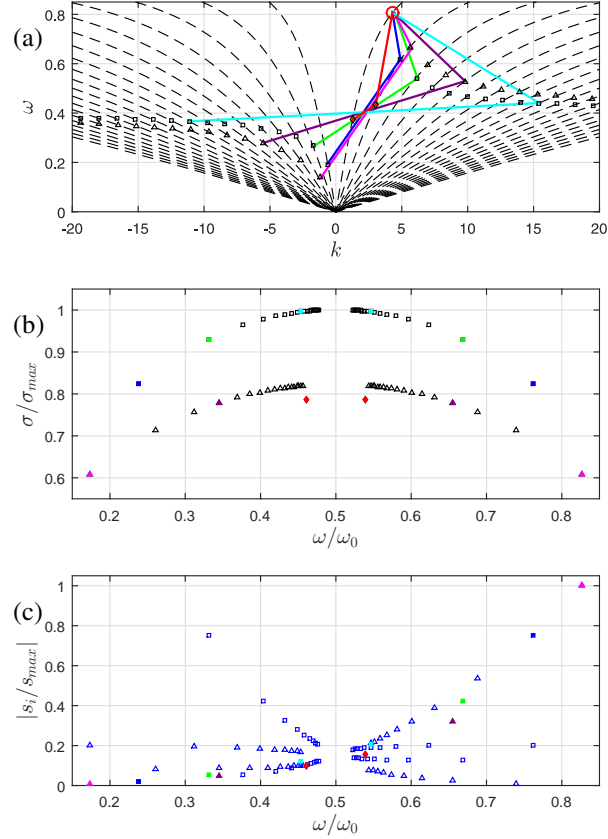


Figure 1: (a) Geometric construction of several of possible triad resonances (c.f. (1)) between a primary internal wave of $\omega=0.8$ (red circle) and pairs of lower harmonic waves for $ah=0.05$. Square and triangles correspond to the higher mode propagating respectively in the same/opposite direction of the primary wave, and diamonds show a special case in which both subharmonic waves travel in the same direction. Six triads are highlighted by color solid lines. Black dashed lines show branches of the dispersion relation $\omega = |k/\sqrt{k^2 + m^2}|$. (b) Variation of the normalized exponent (σ/σ_{max}) of linear stability analysis (7) as a function of normalized frequency ω/ω_0 . Clearly subharmonic waves with frequencies close to $\omega/2$ have the highest exponents [c.f. figure 11b of 21]. (c) Normalized interaction coefficient $|s_i/s_{max}|$ as a function of normalized frequency ω/ω_0 . The maximum initial growth rate occurs at the frequency $\omega/\omega_0=0.83$ although σ is maximum at $\omega/\omega_0=0.5$.

3 Dominant Subharmonic Waves

The subharmonic waves generated in the process of PSI must satisfy the resonant condition (1) and the dispersion relation $\omega = |k/\sqrt{k^2+m^2}|$. As an example of the wave triads satisfying the resonance conditions, for the choice of $ah = 5 \times 10^{-2}$ and $\omega_0 = 0.8$, we present in figure 1a several of possible subharmonic wave triads that can be excited by PSI of the primary wave (red circle). The total number of triad possibilities is (countably) infinite. Note that there are two distinct branches of triads in figure 1a, marked by triangles and squares. Clearly, as the wavenumber of perturbation waves involved in the triad increases the frequency of perturbation waves asymptotically tend to half the frequency of the primary wave ($\omega_0/2$). In other words, perturbation waves with frequencies near $\omega_0/2$ have large horizontal and vertical wavenumbers, i.e., $|k_1, m_1| \approx |k_2, m_2| \gg |k_0, m_0|$ [c.f. e.g. 22].

Based on the linearized instability theory, i.e. assuming that the amplitude of the primary wave is constant (of course this only applies for the very initial period of the resonance), then (4) becomes,

$$dA_1(t)/dt = s_1 A_0 \bar{A}_2(t), \quad (6a)$$

$$dA_2(t)/dt = s_2 A_0 \bar{A}_1(t), \quad (6b)$$

where A_0 is a constant. If the initial amplitudes of the two perturbing waves are respectively $A_1|_{t=0} = \delta_1$ and $A_2|_{t=0} = \delta_2$, the solution to $A_1(t)$ is,

$$\begin{aligned} A_1(t) = & 1/2 \left(\frac{s_1 A_0 \bar{\delta}_2}{\sigma} + \delta_1 \right) \exp(\sigma t) \\ & - 1/2 \left(\frac{s_1 A_0 \bar{\delta}_2}{\sigma} - \delta_1 \right) \exp(-\sigma t) \end{aligned} \quad (7)$$

where $\sigma = \sqrt{s_1 s_2} |A_0|$. A similar expression is obtained for $A_2(t)$ with subscripts 1,2 in (7) swapped.

In classical theory of PSI, σ has been considered as the measure of growth of perturbation waves. We show in figure 1b the plot of σ/σ_{max} (i.e. σ normalized by the maximum σ found from all possible PSI triads) as a function of ω/ω_0 , where ω refers to the frequency of perturbation waves. Colors of markers in figure 1b are associated with the colors of triads depicted geometrically in figure 1a. In each resonance, two perturbation waves are involved that are shown with a pair of same-color markers. For instance, triad of green color occurs between perturbation waves of frequencies $\omega_{1,2}/\omega_0 = 0.34, 0.66$, and results in $\sigma/\sigma_{max} = 0.93$. The two arc-shaped branches formed in this plot correspond to the two branches of triad possibilities in figure 1a (triangles and squares, as discussed before). Behavior of σ presented in figure 1b matches exactly figure 11b of [21] except that in our case because of two horizontal top and bottom boundaries we get discrete modes only.

Clearly figure 1b suggests that the maximum of σ is at $\omega/\omega_0 = 0.5$. But it is to be noted that this does not imply that the initial growth rate nor the long-time growth is highest at $\omega/\omega_0 = 0.5$. Specifically, at large t , it is in fact expected that the exponential term dominates the behavior. However, the linear stability analysis is not valid for large t , and a nonlinear analysis must be called. The linear theory is only applicable at initial times, and the initial growth rate is given by

$$\left. \frac{dA_{1,2}(t)}{dt} \right|_{t=0} = s_{1,2} A_0 \bar{\delta}_{2,1}. \quad (8)$$

Effect of σ in the exponent, as can be seen from (7), is canceled by the coefficients in front, and therefore, the initial growth rate (8), is determined by $s_{1,2}$, and not σ . Behavior of normalized correct initial growth rate s_i/s_{max} plotted against ω/ω_0 (figure 1c) shows almost an opposite behavior when compared with that of σ . Most importantly, the highest value of correct initial growth rate s_{max} , does not occur at $\omega/\omega_0 = 0.5$, but at $\omega/\omega_0 = 0.85$. In fact, perturbation waves with frequencies near $\omega/\omega_0 = 0.5$ have almost the smallest initial growth rates³.

To determine the long term growth of waves involved in PSI, nonlinear stability analysis must be conducted. Since all pairs of perturbation waves (that satisfy resonance condition) simultaneously interact with the primary

³We would like to note that s_i for some of the perturbation waves is negative and therefore the amplitude will first decrease. Usually in such cases, since the amplitude of perturbation waves are initially small, the amplitude quickly decreases to zero and then starts to grow on the negative side. The negative amplitude means that the wave gains a π -radian phase difference.

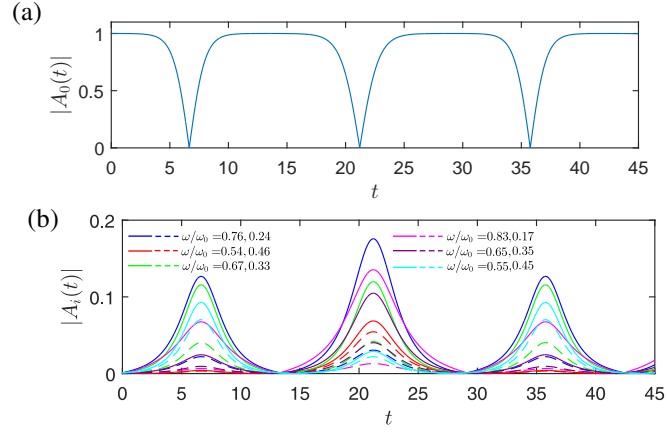


Figure 2: Evolution of amplitudes of (a) the primary internal wave and (b) the six subharmonic pairs undergoing PSI corresponding to the case represented in figure 1. Initial amplitudes of perturbation waves chosen as $A_{i1/i2}|_{t=0}=0.001$ and up to mode 20th (which results in 38 PSI pairs) are considered in the numerical integration of (9). All waves undergo a modulation in time, and the maximum growth is obtained for perturbation wave of $\omega/\omega_0=0.76$.

wave, a correct form of (4) that takes into account the coupling between waves read

$$dA_0(t)/dt = \sum_{i=1}^N s_{i0} A_{i1}(t) A_{i2}(t) \quad (9a)$$

$$dA_{i1}(t)/dt = s_{i1} A_0(t) \bar{A}_{i2}(t) \quad (9b)$$

$$dA_{i2}(t)/dt = s_{i2} A_0(t) \bar{A}_{i1}(t) \quad (9c)$$

where subscript i denotes the i th subharmonic wave pair. From (9), it can be rigorously shown that

$$\frac{d}{dt} \left\{ \frac{|A_0|^2}{\omega_0^2} + \sum_{i=1}^N \left[\frac{|A_{i1}|^2}{\omega_{i1}^2} + \frac{|A_{i2}|^2}{\omega_{i2}^2} \right] \right\} = 0, \quad (10)$$

which shows that our governing equation (9) conserves energy. In other words, although energy is exchanged between a large number of waves, the total energy of the system is conserved and does not change with the time. As a case study, consider a primary internal wave of $\omega_0 = 0.8$ in a stratified water of $ah = 5 \times 10^{-2}$ which is correspond to figure 1. If we consider wave modes up to the mode 20th, that is 20 branches of the dispersion relation plot (dashed lines) in figure 1a, then 38 pair of perturbation waves can be found to form resonance with our primary wave (6 of them are shown in figure 1a). We assume all these perturbation waves have the same initial amplitude $A_i = 1 \times 10^{-3}$, which corresponds to a white-noise-like distribution of perturbation waves in the environment. Results of long time evolution of the primary wave, as well as few important perturbation waves, are shown in figure 2a,b: at the stage $t < 6.8$, amplitudes of some of perturbation waves increase, in cases substantially and even by orders of magnitudes, at the expense of a decrease in the energy of primary wave. Once the entire energy of the primary wave is depleted, then the process reverses and now energy flows back from (initially) perturbation waves to the primary wave. This modulation continues with a period of $T_i \sim 15$ for primary wave and with the period of $T_p \sim 2T_i$ for perturbation waves.

The most important feature of long-time evolution plots (figure 2b) is the fact that the largest growth is observed at frequency $\omega/\omega_0 = 0.76$ ($A_i = 0.18$ at $t=21.7$). The second and third largest growth are respectively at frequency $\omega/\omega_0 = 0.83$ ($A_i = 0.13$ at $t=21.7$) and $\omega/\omega_0 = 0.67$ ($A_i = 0.12$ at $t=21.7$); none at the frequency $\omega/\omega_0 = 0.5$. The perturbation wave associated with $\omega/\omega_0 = 0.55$ (which is closest to 0.5 in our database) gains a maximum value of $A_i = 0.093$ which is barely 50% of the highest growth.

We validate our analytical predictions with direct simulation run by MITgcm [26]. MITgcm is a finite-volume based open-source non-hydrostatic Navier-Stokes solver that is widely used for modeling stratified mediums

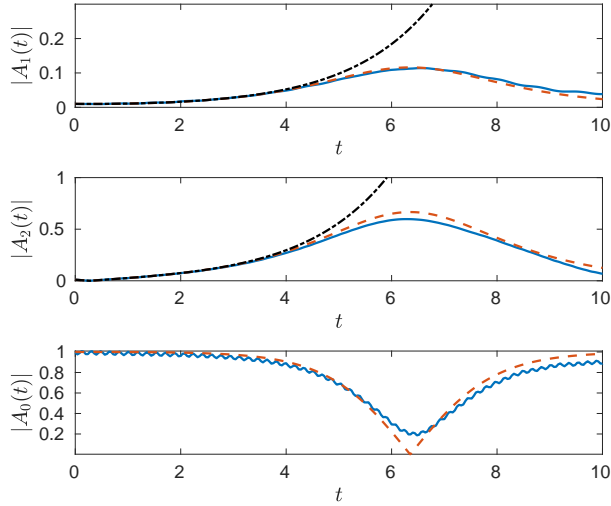


Figure 3: Time-evolution of a primary internal wave of frequency $\omega = 0.8$ with two perturbation waves of frequencies $\omega_{1,2}/\omega_0=0.24,0.76$. Direct simulations results of MITgcm (blue solid line) matches well with our analytical results using nonlinear stability theory though numerical integration of (9) (red dashed line). For comparison, growth rate prediction by linear stability theory (black dash-dotted line) are also shown. Physical parameters for MITgcm simulations are $a = 5 \times 10^{-5}\text{m}^{-1}$, $h = 1000\text{m}$ and initial amplitude is 1m for the primary wave and 0.01m for each of the two subharmonic waves.

[e.g. 27, 28, 29, 30, 31]. We consider a rectangular domain with a periodic boundary condition on both ends in the x-direction, a free-slip wall at the bottom, and a free-slip rigid lid at the top. We use physical parameters $a = 5 \times 10^{-5}\text{m}^{-1}$, $h = 1000\text{m}$ and consider a primary wave of mode one with $\omega_0 = 0.806$, $A_0|_{t=0}=1\text{m}$, that resonates two subharmonic waves of frequencies $\omega_{1,2}/\omega_0 = 0.24, 0.76$, $A_{1,2}|_{t=0}=0.01\text{m}^4$. The evolution of amplitude of the three waves over time obtained from the direct simulation of MITgcm (blue solid lines in figure 3) compares well with our analytical results obtained from (9) (red dashed curves). For comparison, we also show the results of linear stability analysis (black dash-dotted lines) on top of the other two curves. Clearly, at the initial stage of resonance and as long as the change in the amplitude of A_0 is small, linear stability analysis estimates the growth of perturbations with a satisfactory tolerance. But for later stages, linear theory over-predicts the growth.

4 Conclusion

In summary, we showed, contrary to widely-accepted results drawn from linearized instability theory, that Parametric Subharmonic Instability (PSI) is strongest among a primary internal waves and perturbation waves at frequencies different from half the frequency of internal wave. Specifically, we proved that both the initial growth rate and the maximum amplitude reached by the (initially) perturbation waves are highest for subharmonic waves of low vertical modes with frequencies higher than $\omega_0/2$. It is straightforward to show that similar conclusion holds also in the spatial (or boundary value) problem, i.e. as waves propagate away from a source (e.g. a wavemaker) and interaction develops over the distance [c.f. e.g. 32]. Our finding suggests that the efficiency of converting internal wave energy from large scales to small scales through PSI may have been overestimated by previous studies, and dominant resonant waves may have been missed if sought at the half frequency.

⁴This specific pair of subharmonics are intentionally chosen since their wavenumber are $k_{1,2}/k_0=-1/7,8/7$ allowing us to use a periodic domain in the x-direction.

References

- [1] Carl Wunsch and Raffaele Ferrari. Vertical mixing, energy, and the general circulation of the oceans. *Annu. Rev. Fluid Mech.*, 36:281–314, 2004.
- [2] Chris Garrett. Internal tides and ocean mixing. *Science (New York, N.Y.)*, 301(5641):1858–9, 2003.
- [3] Philip W. Boyd. Biogeochemistry: Iron findings. *Nature*, 446(7139):989–991, 2007.
- [4] Graham P. Harris. Chapman and Hall, 1986.
- [5] Kevin G Lamb. Internal Wave Breaking and Dissipation Mechanisms on the Continental Slope/Shelf. *Annual Review of Fluid Mechanics*, 46:231–54, 2014.
- [6] S. Sarkar and A. Scotti. From topographic internal gravity waves to turbulence. *Annual Review of Fluid Mechanics*, 49(1):195–220, 2017.
- [7] Likun Zhang and Harry L. Swinney. Virtual seafloor reduces internal wave generation by tidal flow. *Phys. Rev. Lett.*, 112:104502, 2014.
- [8] K. Hasselmann. A criterion for nonlinear wave stability. *Journal of Fluid Mechanics*, 30(04):737, 1967.
- [9] R E Davis and A Acrivos. The stability of oscillatory internal waves. *Journal of Fluid Mechanics*, 30(4):723–736, 1967.
- [10] H el ene Scolan, Eugeny Ermanyuk, and Thierry Dauxois. Nonlinear fate of internal wave attractors. *Phys. Rev. Lett.*, 110:234501, 2013.
- [11] Peter N Lombard and James J Riley. Instability and breakdown of internal gravity waves. I. Linear stability analysis. *Physics of Fluids*, 8:3271–3287, 1996.
- [12] Hussain H Karimi and T R Akylas. Parametric subharmonic instability of internal waves: locally confined beams versus monochromatic wavetrains. *Journal of Fluid Mechanics*, 757:381–402, 2014.
- [13] C. R. Koudella and C. Staquet. Instability mechanisms of a two-dimensional progressive internal gravity wave. *Journal of Fluid Mechanics*, 548:165, 2006.
- [14] Thierry Dauxois, Sylvain Joubaud, Philippe Odier, and Antoine Venaille. Instabilities of Internal Gravity Wave Beams. *Annual Review of Fluid Mechanics*, 50:1–28, 2018.
- [15] M Phillip. Wave interactions - the evolution of an idea. *Journal of Fluid Mechanics*, 106:215–227, 1981.
- [16] Chung-Hsiang Jiang and Philip S. Marcus. Selection rules for the nonlinear interaction of internal gravity waves. *Phys. Rev. Lett.*, 102:124502, 2009.
- [17] M. H. Alford. Observations of parametric subharmonic instability of the diurnal internal tide in the South China Sea. *Geophysical Research Letters*, 35(15):2–6, 2008.
- [18] Brian S. Chinn, James B. Girton, and Matthew H. Alford. Observations of internal waves and parametric subharmonic instability in the Philippines archipelago. *Journal of Geophysical Research: Oceans*, 117(5):1–12, 2012.
- [19] S. Martin, W. Simmons, and C. Wunsch. The excitation of resonant triads by single internal waves. *Journal of Fluid Mechanics*, 53:17–44, 1972.
- [20] A. D. McEwan. Degeneration of resonantly-excited standing internal gravity waves. *Journal of Fluid Mechanics*, 50(03):431–448, 1971.
- [21] Baptiste Bourget, Thierry Dauxois, Sylvain Joubaud, and Philippe Odier. Experimental study of parametric subharmonic instability for internal plane waves. *Journal of Fluid Mechanics*, 723:1–20, 2013.

- [22] C. Staquet and J. Sommeria. Internal gravity waves : from instabilities to turbulence. *Annual Review of Fluid Mechanics*, 34:559–593, 2002.
- [23] Sylvain Joubaud, James Munroe, Philippe Odier, and Thierry Dauxois. Experimental parametric subharmonic instability in stratified fluids. *Physics of Fluids*, 24(24):41703–23116, 2012.
- [24] Alexander S. Korobov and Kevin G. Lamb. Interharmonics in internal gravity waves generated by tide-topography interaction. *J. Fluid Mech*, 611:61–95, 2008.
- [25] A. D. McEwan, D. W. Mander, and R. K. Smith. Forced resonant second-order interaction between damped internal waves. *Journal of Fluid Mechanics*, 55(04):589, 1972.
- [26] J. Marshall, A. Adcroft, C. Hill, L. Perelman, and C. Heisey. A finite-volume, incompressible Navier Stokes model for studies of the ocean on parallel computers. *Journal of Geophysical Research*, 102:5753–5766, 1997.
- [27] A. Engqvist and A.M. Hogg. Unidirectional stratified flow through a non-rectangular channel. *J. Fluid Mech.*, 509:83–92, 2004.
- [28] J. M. Klymak, S. M. Legg, and R. Pinkel. High-mode stationary waves in stratified flow over large obstacles. *Journal of Fluid Mechanics*, 644:321–336, 2010.
- [29] K. Lim, G. N. Ivey, and N. L. Jones. Experiments on the generation of internal waves over continental shelf topography. *Journal of Fluid Mechanics*, 663:385–400, 2010.
- [30] E. N. Churaev, S. V. Semin, and Y. A. Stepanyants. Transformation of internal waves passing over a bottom step. *Journal of Fluid Mechanics*, 768:1–11, 2015.
- [31] Matthew H. Alford, Thomas Peacock, and Jennifer A. MacKinnon et al. The formation and fate of internal waves in the South China Sea. *Nature*, 521(7550):65–69, 2015.
- [32] Mohammad-Reza Alam, Yuming Liu, and Dick KP Yue. Bragg resonance of waves in a two-layer fluid propagating over bottom ripples. part ii. numerical simulation. *Journal of Fluid Mechanics*, 624:225–253, 2009.